Contents

1 Comparative analysis:

Features	HCCNC	Streamwise CCNC	Why it matters
Stable supersaturation levels (%)	0.05-2[#]	0.13[+]-2	Extends measurements to lower SS and larger dry diameters across all aerosol types
Temperature (°C) at which supersaturation can be generated	4-40	30[*]-52	May better preserve semi-volatile components
No loss of data during SS cycle	✓	× Stabilization required after SS steps (sec. to min.)	Improves usable time resolution in rapidly changing air masses
Dynamic residence time (seconds)	8–24	6-12	Will enable kinetic growth studies at different T and SS
Easy to change water vapor source (whisk or filter paper) after intense measurement campaign	✓ (3 steps process)		Shorter downtime; modular parts

[#]: efforts are underway to push this limit higher.

[+]: 0.2% in some cases,

*: Assuming sample temperature equal to 25°C and stable supersaturation (i.e. > 0.13%)

2 The low-supersaturation wall

2.1 Theoretical foundation

Note on what follows

The values presented in this subsection are derived solely through the κ-Köhler equation[1], not from direct in-situ measurements (expect ammonium sulphate). They are mathematical predictions intended to illustrate the size of the measurement gap that the HCCNC architecture could help close. The experimental validity of this framework was demonstrated for 200 nm particles[3], establishing a baseline for instrument response in the regime of interest.

The relationship between a particle's hygroscopicity (κ), its dry diameter (D_d), and the critical supersaturation (S_c) required for activation is described by the simplified κ-Köhler equation[1]:

$$S_c = sqrt\left(\frac{(4\,A^3)}{(27\,k\,D_d^3)}\right), A = \frac{(4\,\sigma_w M_w)}{(R\,T\,\rho_w)} \quad 1$$

Here, A is the Kelvin term, computed from the properties of pure water at standard conditions ($\sigma_w \approx 0.072$ J m^{-2}, T = 298.15 K). The critical supersaturation S_c is related to the instrument's percentage supersaturation by SS = (S_c – 1) × 100 %.

Inverting the equation to solve for D_d at a fixed κ and the minimum stable SS achievable by a given instrument yields the instrument's measurement "ceiling." This calculation establishes the theoretical activation threshold for representative aerosol regimes (SOA, marine, continental) drawn from the literature[1,2].

Applying this framework to quasi-monodisperse aerosol populations illustrates the lower operational limits of streamwise CCNC. Assuming a highly soluble aerosol (κ = 0.92), the theoretical S_c for a 50 nm particle is calculated to be 0.34%. However, because solute volume scales cubically with dry diameter, a 150 nm particle of identical composition activates at a much lower S_c of just 0.065%.

To visualize this size-dependent behavior against instrument parameters, idealized size distributions (Fig. 1a) and their corresponding sigmoidal Activation Fraction (AF) curves (Fig. 1b) were theoretically generated. The activation curves were modeled using the cumulative error function, which maps the lognormal geometric standard deviation of the assumed size distribution ($\sigma_g = 1.08$) into supersaturation space ($\sigma_{g,SS} = \sigma_g^{1.5}$):

$$AF(SS) = \frac{1}{2}\left[1 + \mathrm{erf}\left(\frac{\ln(SS/SS_{crit})}{\sqrt{2}\ln(\sigma_{g,SS})}\right)\right]$$

The resulting simulation underscores the experimental constraints encountered when analyzing larger or highly hygroscopic particles. The 50 nm activation curve is fully resolved within the instrument's reliable supersaturation regime (>0.13%), allowing for

accurate retrieval of the inflection point (AF = 0.5)—the 150 nm curve falls entirely below this threshold. By the time the instrument reaches its lowest stable operating setpoint, the 150 nm population is already fully activated. This yields a truncated plateau that obscures the vital rising edge of the S-curve, preventing the mathematical extraction of its true S_c.

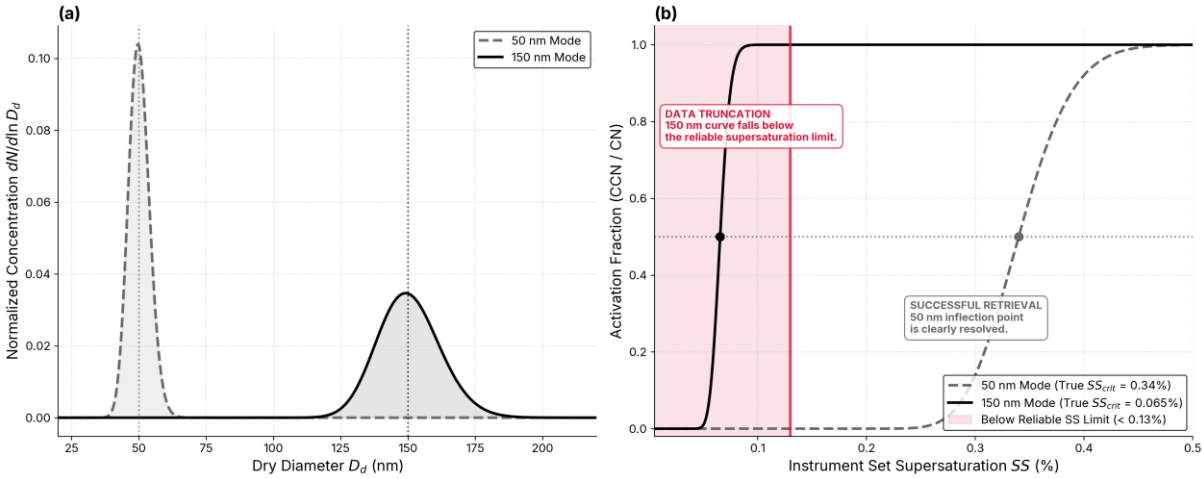

Figure 1. (a) Idealized size distributions for quasi-monodisperse 50 nm and 150 nm aerosol populations ($\sigma_g = 1.08$). (b) Corresponding sigmoidal activation fraction curves mapped against instrument supersaturation. The red shaded region represents the standard CCNC's unstable operating regime (SS < 0.13). *(Modeled prediction based on κ-Köhler theory).*

2.2 Another Example: Pristine Southern Ocean

Applying the streamwise CCNC's 0.13% operational limit to a Southern Ocean (κ = 0.92) establishes a maximum resolvable dry diameter of 96 nm. When evaluated against a representative Southern Ocean size distribution taken from Alroe, J. et al.[4], a measurement gap could emerge (Fig. 2). The primary accumulation mode peaks at 121 nm (activating at 0.09%). Because this falls below the standard instrument's stable floor, the vital sigmoidal rise could be lost, risking biased κ_{sup} retrievals from the resulting truncated data.

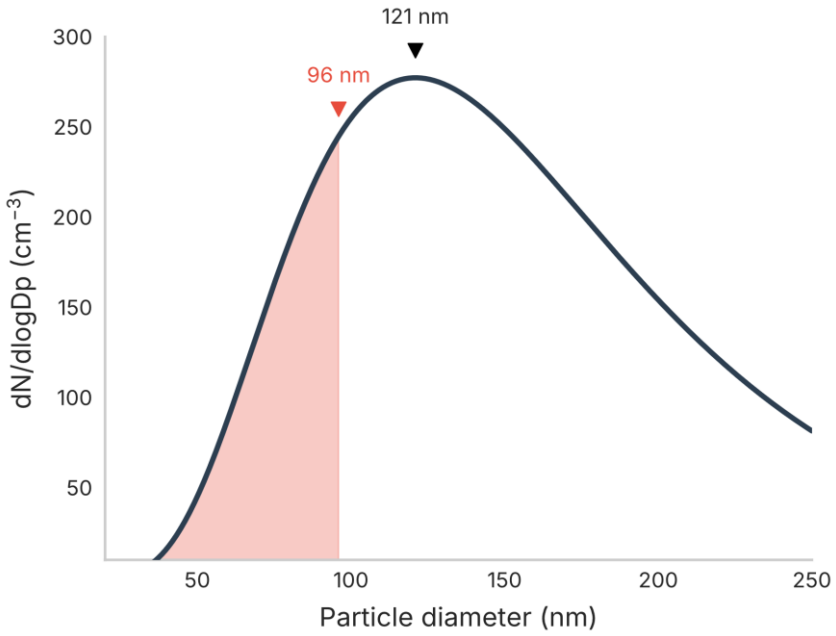

Figure 2. Simulated pristine Southern Ocean dry-number size distribution. The pink-shaded region denotes the maximum particle size (D_d = 96 nm) reliably resolvable by the standard CCNC, which misses the 121 nm accumulation peak.

In contrast, extended-range instruments like the HCCNC achieve stable supersaturations down to 0.05%, pushing the resolvable diameter ceiling to 181 nm (Fig. 3). This expanded range nearly doubles the accessible sizes, successfully capturing almost the entire accumulation mode.

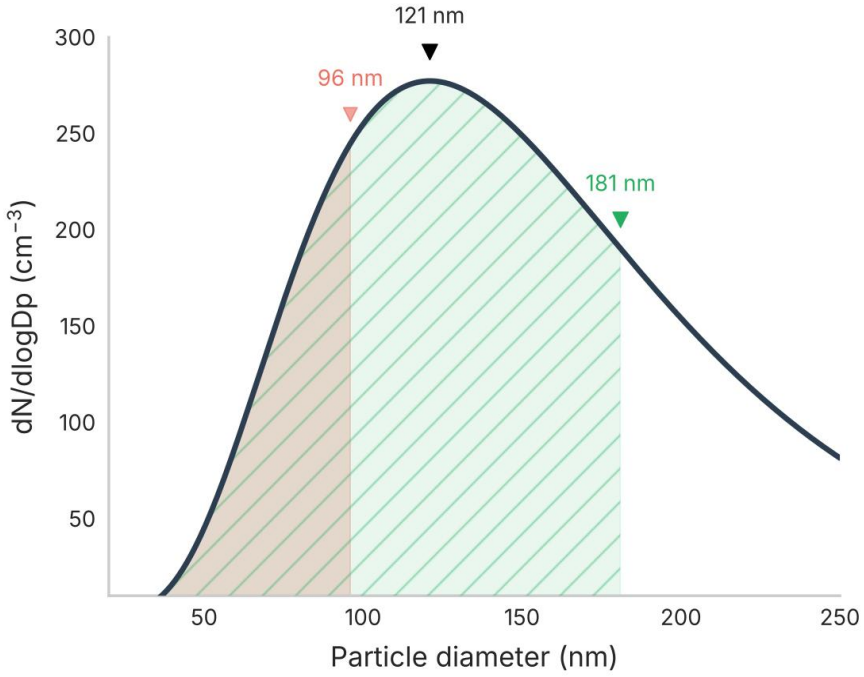

Figure 3. The Southern Ocean size distribution comparing the operational range of the HCCNC (green hatched, D_d = 181 nm) against the standard CCNC (pink hatched; *modeled prediction based on κ-Köhler theory).*

2.3 Across Compositions: The ~2× Rule

The Southern Ocean example represents just a single composition. However, the geometric advantage of the HCCNC's lowered supersaturation floor applies theoretically universally. By taking the ratio of the critical diameters at the two instrument limits, the composition-dependent terms (hygroscopicity κ, surface tension, and temperature) cancel out entirely:

$$\frac{D_{HCCNC}}{D_{DMT}} = \left(\frac{0.13}{0.05}\right)^{\frac{2}{3}} \approx 2$$

This reveals that the HCCNC can access dry diameters nearly twice as large as the standard CCNC . This expansion ratio is dictated exclusively by the instrument supersaturation limits, rendering it completely independent of aerosol composition.

Table 1. Critical activation diameters (D_c) at the 0.13% (streamwise CCNC) and 0.05% (HCCNC) supersaturation limits across six representative κ regimes.

κ regime	κ	D_c @ 0.13%	D_c @ 0.05%	Source
Sodium chloride	1.28	86 nm	163 nm	Petters & Kreidenweis (2007)[1]

Southern Ocean	0.92	96 nm	181 nm	Pringle et al. (2010)[2]
Marine background (global)	0.72 ± 0.24	104 nm	197 nm	Pringle et al. (2010)[2]
Ammonium sulfate (CCN-derived)	0.61	110 nm	208 nm	Petters & Kreidenweis (2007)[1]
Continental ambient (global)	0.27 ± 0.21	145 nm	273 nm	Pringle et al. (2010)[2]
Secondary organic aerosol	0.10	201 nm	380 nm	Petters & Kreidenweis (2007)[1]

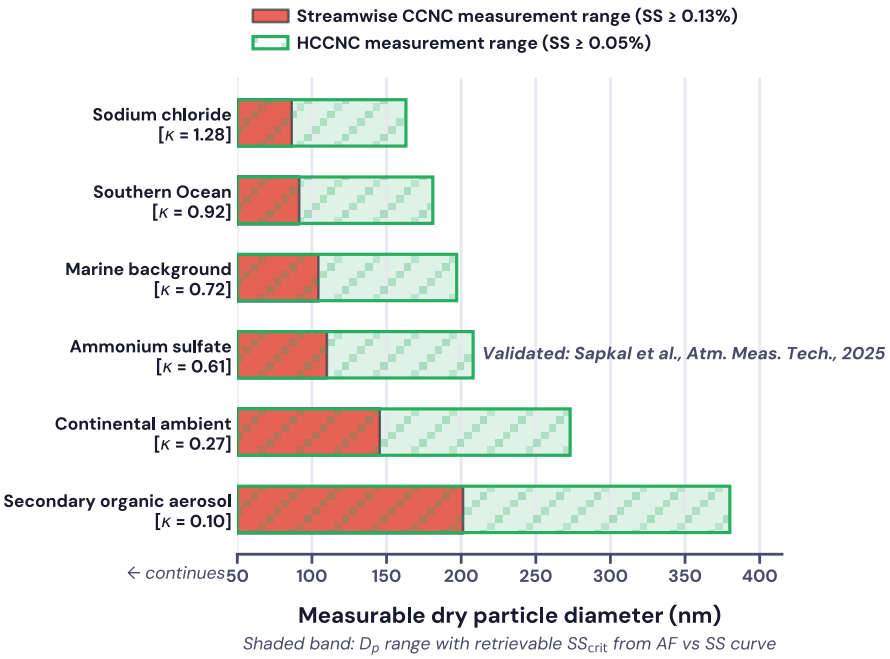

Figure 4. Critical activation diameters at the streamwise CCNC (0.13%, red) and HCCNC (0.05%, green) operational floors across six κ regimes, spanning about two orders of magnitude in hygroscopicity. The expansion of the measurement range follows the universal ~2× scaling rule. For pristine marine aerosol, the HCCNC unlocks diameters from 96 nm up to 181 nm; for continental aerosol, 145 nm to 273 nm; and for SOA, 201 nm to 380 nm. *(Modeled prediction based on κ-Köhler theory, measurements have been done for the ammonium sulphate for HCCNC only).*

References

1. Petters, M. D. & Kreidenweis, S. M. A single parameter representation of hygroscopic growth and cloud condensation nucleus activity. Atmos. Chem. Phys. 7, 1961–1971 (2007).
2. Pringle, K. J., Tost, H., Pozzer, A., Pöschl, U. & Lelieveld, J. Global distribution of the effective aerosol hygroscopicity parameter for CCN activation. Atmos. Chem. Phys. 10, 5241–5255 (2010).
3. Sapkal, M. G., Rösch, M. & Kanji, Z. A. Development and validation of a horizontal CCN counter operating at low temperature and supersaturation. Atmos. Meas. Tech. 18, 5649–5672 (2025).
4. Alroe, J. et al. Marine productivity and synoptic meteorology drive summer-time variability in Southern Ocean aerosols. Atmos. Chem. Phys. 20, 8047–8062 (2020).